IEEE Access
Multidisciplinary | Rapid Review | Open Access Journal

Received March 28, 2020, accepted April 6, 2020, date of publication April 14, 2020, date of current version April 29, 2020.

Digital Object Identifier 10.1109/ACCESS.2020.2987912

Variable Pitch Active Disturbance Rejection Control of Wind Turbines Based on BP Neural Network PID

HAIJUN REN, BIN HOU, GAO ZHOU, LI SHEN, CHONG WEI, AND QI LI
School of Advanced Manufacture Engineering, Chongqing University of Posts and Telecommunications, Chongqing 400065, China

Corresponding author: Haijun Ren (renhj@cqupt.edu.cn)

This work was supported by the National Natural Science Fund of China under Grant 51405052.

ABSTRACT When wind speeds are above the rated speed of variable speed variable pitch wind turbines, pitch angles are changed to keep output powers and rotor speeds at their rated values. For wind turbines with nonlinear and complex structure, conventional PID variable pitch controller is difficult to achieve precise control. In this paper, a variable pitch controller combining back-propagation(BP) neural network with PID (BP-PID) is proposed. By real-time detecting the deviation of the rotor speeds, the BP neural network with self-learning and weighting coefficient correction capability is used to adjust the PID parameters online and further to achieve the optimal combination of the PID parameters. Considering various uncertain disturbances and parameter changes on the mechanical components of the wind turbines, an active disturbance rejection pitch controller of the wind turbines is designed based on BP-PID algorithm. Combined with a tracking differentiator, an extended state observer (ESO) is employed to observe the state and disturbance of the system. In addition, in order to compensate the BP-PID variable pitch controller, nonlinear state error feedback control laws are designed by configuring nonlinear structures according to the state deviation between the extended state observer and the tracking differentiator. The simulation results show that the variable pitch active disturbance rejection control (ADRC) based on BP-PID can effectively estimate the system states and disturbances. And the proposed controller has good dynamic performance and strong robustness.

INDEX TERMS Wind turbine, pitch control, BP-PID, active disturbance rejection control, extended state observer.

I. INTRODUCTION

With the rapid advancement of wind power technology, wind power has become one of the fastest growing power industries all over the world [1]. Wind turbines have evolved from the initial fixed pitch to the variable pitch and further from the variable pitch with fixed speed to the current variable speed variable pitch. Accordingly, the power generation efficiency is significantly improved. Variable speed variable pitch wind turbines extract the maximum power by increasing wind power coefficient at low wind speeds and variable pitch control strategies are used at high wind speeds to keep output powers at the rated value [2]–[6]. At different wind conditions, the operating regions of the wind turbine are generally divided into four parts. In region 1, the actual wind speed is less than the cut-in wind speed of the wind turbine, which the wind turbine is in shutdown state. In region 2, the wind speed is between the cut-in wind speed and the rated wind speed, which the generator torque control is adopted to make the generator rotor speed change with the wind speed, thereby obtaining the maximum wind power conversion efficiency. In region 3, the wind speed is between the rated wind speed and the cut-out wind speed. As high wind speeds can damage wind turbines, pitch technologies are adopted to ensure output powers of the wind turbines at the rated value. In region 4, the wind speed is over the cut-out value. During this region, in order to prevent the wind turbine from being damaged, the pitch angle is set to 90 degree [7]–[15]. This paper focuses on the pitch control strategy for region 3.

In recent years, many scholars have designed different control algorithms for wind turbine pitch systems [16]–[23]. Ref. [16] proposed a wind turbine control strategy that directly

The associate editor coordinating the review of this manuscript and approving it for publication was Gaolin Wang.

drives a permanent magnet synchronous generator without a wind speed sensor, in which a power smoothing strategy was adopted in the high wind speed region to optimize the output power. Ref. [17] proposed a pitch control strategy based on particle swarm optimization algorithm. Simulation results show that the new algorithm has a good regulation effect on the rotor speeds and output powers of the wind turbine. For considering the disturbances in actual wind speeds, Ref. [18] proposed a variable pitch control strategy with anti-interference capability. According to the Hamilton-Jacobi-Bermann equation, the feedback and feedforward control term functions are derived for stabilizing the wind turbine system and suppressing wind disturbance. So the speed regulation and steady-state error adjustment are better achieved. As it is possible to limit the active power and rotor speed of doubly-fed induction generators at high wind speeds, Refs. [19], [20] designed a fractional-order PI controller, which used fractional-order coefficients as additional control variable and was applied to the pitch angle compensation control loop. Accordingly, doubly-fed induction generator active powers were improved and rotor speeds were optimized. Ref. [21] proposed a new method to reduce the error in the pitch angle measurement, which uses the laser scanner to measure the pitch angle. The case study shows the effectiveness of the pitch angle measurement method. Ref. [22] proposed a cooperative fault-tolerant control strategy to compensate the faults generated by the pitch angle actuator. By designing an adaptive cooperative observer and a reconfigurable controller, the fault of the pitch angle actuator can be estimated. In order to improve the controllability and stability of the pitch system, Ref. [23] designed a two-degree-of-freedom motion control pitch angle controller combined with feedback linearization to overcome the nonlinearity of the system. However, under actual wind conditions, the structural parameters and external disturbances of the wind turbine are often changing. Most of the above mentioned wind turbine pitch control strategies depend on the accurate mathematical model of the system, and the solution to the system interference is simple.

In this paper, an active disturbance rejection pitch control strategy based on BP-PID is proposed to improve the performance of the controller and ensure that the rotor speed and output power are kept at their rated values in the high wind speed region. In the feedback loop, the BP-PID pitch controller is designed, which uses the rotor speed deviation signal as the control variable and real-time adjusts the weighting coefficients by its self-learning [24]–[29]. Considering the changes of wind turbine structural parameters and system disturbances under actual wind conditions, an ADRC algorithm [30]–[38] is proposed to observe system state changes and disturbances and further to realize compensation of the BP-PID pitch controller. The simulation experiments show that the variable pitch active disturbance rejection controller based on BP-PID has stronger stability, faster response speed and better robustness than those of the BP-PID pitch controller.

II. WIND TURBINE SYSTEM MODELLING

A wind turbine is a device that converts wind energy into electrical energy. The mechanical power and mechanical torque obtained by the wind turbine are as follows [32].

$$P_w = 0.5\rho\pi R^2 V^3 C_p(\lambda,\theta) \tag{1}$$

$$T_w = P_w/\omega_r = \rho\pi R^2 V^3 C_p(\lambda,\theta)\Big/2\omega_r \tag{2}$$

where P_w is the mechanical energy captured by the wind turbine, T_w is the mechanical torque generated by the wind wheel, ρ is the air density, R is the radius of the wind wheel, V is the upstream wind speed of the wind wheel, θ is the pitch angle, ω_r is the rotor speed, and $C_p(\lambda,\theta)$ is the wind power coefficient.

The wind power coefficient is closely related to the structure of blades. The coefficient can be described as follows [17].

$$C_p(\lambda,\theta) = c_1\left(\frac{c_2}{\lambda_t} - c_3\theta - c_4\right)e^{-\frac{c_5}{\lambda_t}} + c_6\lambda \tag{3}$$

where

$$\lambda_t = \frac{1}{\lambda + 0.08\theta} - \frac{0.035}{\theta^3 + 1} \tag{4}$$

$$\lambda = \frac{\omega_r R}{V} \tag{5}$$

where λ is the tip speed ratio, λ_t is the intermediate variable.

The transmission system model near the low-speed shaft side of the wind wheel is as follows.

$$J_w\frac{d\omega_r}{dt} = T_w - T_D - \gamma T_m \tag{6}$$

$$T_D = s_1 + s_2/\omega_r + s_3\omega_r \tag{7}$$

where J_w is the moment of inertia of the wind wheel, T_D is the resistance torque, s_1, s_2, s_3 are the resistance torque coefficients, γ is the gear transmission ratio, T_m is the torque transmitted to the gear by the high speed shaft.

The transmission system model near the high-speed shaft side of the generator is as follows [13].

$$J_g\frac{d\omega_g}{dt} = T_m - T_{em} \tag{8}$$

where J_g is the generator moment of inertia, ω_g is the generator speed, T_{em} is the generator electromagnetic torque.

Substituting $\omega_g = \gamma\omega_r$ and formula (8) into formula (6), the mathematical expression of the transmission system near the rotor side is as follows.

$$(J_w + \gamma^2 J_g)\frac{d\omega_r}{dt} = T_w - T_D - \gamma T_{em} \tag{9}$$

According to the equivalent circuit of the doubly-fed generator and the equations of the stator and rotor, the electromagnetic torque expression is as follows [12].

$$\begin{aligned} T_{em} = {} & \frac{-3spx_m^2 r_2}{\omega_1 c^2}U_1^2 + \frac{3px_m^2 r_1}{\omega_1 c^2}U_2^2 \\ & + \frac{3px_m}{\omega_1 c^2}[(r_1 r_2 + sx_{2\sigma}x_{1\sigma} + sx_m^2)\sin\alpha_{12} \\ & - (sx_{2\sigma}r_1 - x_{1\sigma}r_2)\cos\alpha_{12}]U_1 U_2 \end{aligned} \tag{10}$$

where

$$c = \sqrt{(r_1 r_2 - s x_{2\sigma} x_{1\sigma} + s x_m^2)^2 + (s x_{2\sigma} r_1 + x_{1\sigma} r_2)^2} \quad (11)$$

where p is the pole number, ω_1 is the synchronous angular velocity, s is the slip ratio, U_1 is the stator voltage, U_2 is the rotor voltage, α_{12} is the voltage phase difference between the stator and rotor, r_1 is the resistance of the stator winding, $x_{1\sigma}$ is the leakage reactance of the stator winding, r_2 is the resistance of the rotor winding to the stator side, $x_{2\sigma}$ is the leakage reactance of the rotor winding to the stator side, and x_m is the excitation reactance.

The electromagnetic power of the doubly-fed generator is calculated as follows [13].

$$\begin{aligned} P_e = T_{em}\Omega_1 = {} & \frac{-3s x_m^2 r_2}{c^2} U_1^2 + \frac{3x_m^2 r_1}{c^2} U_2^2 \\ & + \frac{3x_m}{c^2}[(r_1 r_2 + s x_{2\sigma} x_{1\sigma} + s x_m^2)\sin\alpha_{12} \\ & - (s x_{2\sigma} r_1 - x_{1\sigma} r_2)\cos\alpha_{12}] U_1 U_2 \end{aligned} \quad (12)$$

where P_e is the electromagnetic power of the doubly-fed generator, Ω_1 is the synchronous mechanical angular velocity of the generator, $\Omega_1 = \omega_1 / p$.

The wind turbine pitch actuator can be regarded as a first-order inertia expression as follows.

$$\dot{\theta} = \frac{1}{T_\theta}(\theta_r - \theta) \quad (13)$$

where T_θ is the time constant, θ_r is the reference pitch angle.

Based on these analyses, the wind turbine can be expressed as a second-order system as follows.

$$\begin{cases} \dfrac{d\theta}{dt} = \dfrac{1}{T_\theta}(\theta_r - \theta) \\ \dfrac{d\omega_r}{dt} = \dfrac{1}{(J_w + \gamma^2 J_g)}[T_w(V, \theta, \omega_r) \\ \qquad - T_D(\omega_r) - \gamma T_{em}(\omega_r)] \end{cases} \quad (14)$$

The pitch angle θ and rotor speed ω_r are selected as state variables as follows.

$$x = \begin{bmatrix} x_1 \\ x_2 \end{bmatrix} = \begin{bmatrix} \theta \\ \omega_r \end{bmatrix} \quad (15)$$

The reference pitch angle θ_r is selected as the control input of the wind turbine, which is $u = \theta_r$. Then the wind turbine state equation is expressed as follows.

$$\begin{cases} \dfrac{dx_1}{dt} = \dfrac{1}{T_\theta} u - \dfrac{1}{T_\theta} x_1 \\ \dfrac{dx_2}{dt} = \dfrac{1}{(J_w + \gamma^2 J_g)} \times [T_w(V, x_1, x_2) \\ \qquad - T_D(x_2) - \gamma T_{em}(x_2)] \end{cases} \quad (16)$$

The output equation is as follows.

$$y = P_e(x_2) \quad (17)$$

The parameters of the wind turbine are shown in TABLE 1.

TABLE 1. Wind turbine parameters.

Symbol	Parameter	Value
P_r	Rated output power	3MW
V_r	Rated wind speed	12m/s
R	Radius of the rotor	47.5m
J_w	Inertia moment of the rotor	6250000 $\mathrm{kg \cdot m^2}$
J_g	Inertia moment of the generator	15 $\mathrm{kg \cdot m^2}$
γ	Transmission ratio	80
r_1	Stator winding resistance	0.0184 Ω
r_2	Rotor winding resistance calculated to stator	0.0370 Ω
$x_{1\sigma}$	Leakage reactance	0.0727 Ω
$x_{2\sigma}$	Leakage calculated to stator side	0.0863 Ω
x_m	Excitation reactance	2.0000 Ω
s_1	First resistance torque factor	1000
s_2	Second resistance torque factor	1000
s_3	Third resistance torque coefficient	100

III. ACTIVE DISTURBANCE REJECTION COMPOSITE PITCH CONTROL BASED ON BP-PID

For wind turbine systems with the nonlinearity, time-varying and structural complexity, a composite pitch control strategy is proposed, which combines BP-PID with active disturbance rejection control. In the feedback control loop, the BP-PID pitch controller is designed. BP neural network learns the deviations of itself and adjusts the weights of the output layer and hidden layer, which realize the online adjustment of PID parameters. As the BP neural network algorithm has a slower convergence speed and weaker anti-interference capability, an active disturbance resistant pitch control algorithm is proposed based on BP-PID.

Combined with a tracking differentiator, an extended state observer is adopted to estimate the unmodeled part, internal and external disturbances of the wind turbine system. According to the state deviation, an active disturbance rejection controller with nonlinear structure is implemented to compensate the BP-PID pitch controller. The composite pitch control strategy is shown in FIGURE 1.

A. DESIGN OF WIND TURBINE PITCH CONTROLLER FOR BP-PID

BP neural network uses the gradient search technique to continuously correct the weights in the network according to the deviation $e(k)$ between the expected and actual values of the system, until the deviation $e(k)$ reaches the minimum value [25]. Through its self-learning and weighting coefficient correction, BP neural network adjusts the parameters of the PID controller in real time to achieve the optimal combination of

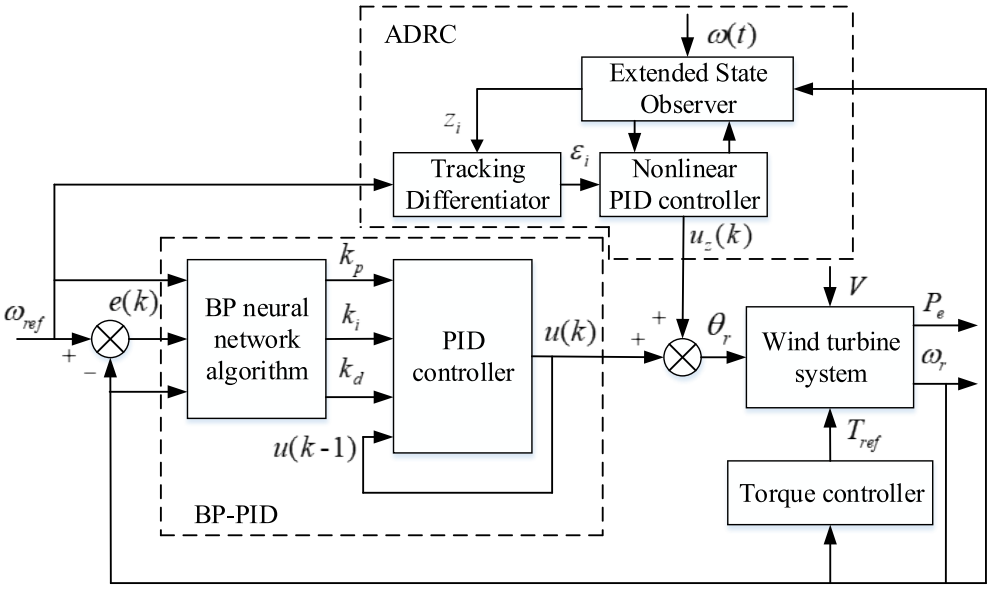

FIGURE 1. The block diagram of the variable pitch control strategy of wind turbine.

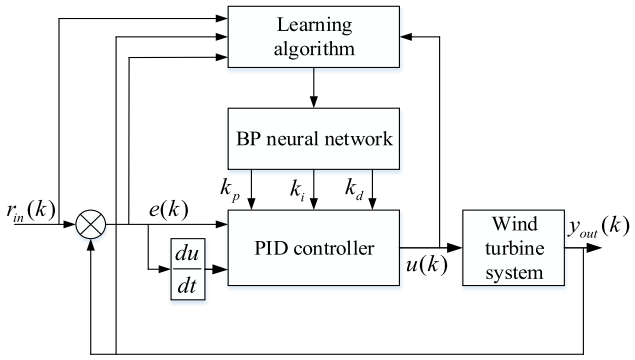

FIGURE 2. The structure diagram of BP-PID controller.

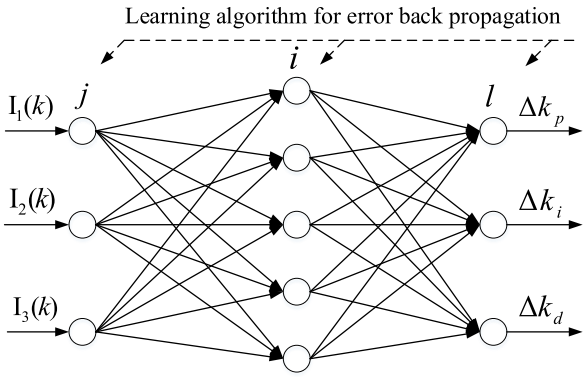

FIGURE 3. BP structure design.

PID parameters. The structure of the controller based on BP-PID is shown in FIGURE 2.

The classic incremental digital PID control algorithm is as follows [26].

$$u(k) = u(k-1) + \Delta u(k) \tag{18}$$

$$\begin{aligned}\Delta u(k) = {} & k_p(k) \cdot [e(k) - e(k-1)] + k_i(k) \cdot e(k) \\ & + k_d(k) \cdot [e(k) - 2e(k-1) + e(k-2)]\end{aligned} \tag{19}$$

where $u(k)$ is the total control input of the controlled system, $\Delta u(k)$ is the control increment from the PID controller, $k_p(k)$, $k_i(k)$ and $k_d(k)$ are proportional, integral, and differential coefficients, respectively. Next, these three parameters are adjusted online by designing the BP neural network algorithm.

1) BP STRUCTURE

This paper uses a 3-layer BP network, which is 3-5-3 structure shown in FIGURE 3. The number of input layer neural units is three, which expectation value is $\mathrm{I}_1(k)$, actual output is $\mathrm{I}_2(k)$, and deviation is $\mathrm{I}_3(k)$, respectively. The hidden layer neurons are five. The output layer neurons are three, which are Δk_p, Δk_i, and Δk_d, respectively.

The three inputs of BP neural network have the following relationship with the expected value and the actual sample value as follows.

$$\begin{cases} \mathrm{I}_1(k) = r_{in}(k) \\ \mathrm{I}_2(k) = y_{out}(k) \\ \mathrm{I}_3(k) = r_{in}(k) - y_{out}(k) \end{cases} \tag{20}$$

where $r_{in}(k)$ is the expected value of the rotor speed, and $y_{out}(k)$ is the actual value of the rotor speed.

Select the appropriate initial parameters $k_p(0)$, $k_i(0)$, $k_d(0)$, then the parameters of BP neural network after each tuning

operation are modified as follows.

$$\begin{cases} k_p(k) = k_p(k-1) + \Delta k_p(k) \\ k_i(k) = k_i(k-1) + \Delta k_i(k) \\ k_d(k) = k_d(k-1) + \Delta k_d(k) \end{cases} \tag{21}$$

2) THE FLOW OF BP-PID CONTROL ALGORITHM

The calculation process can be summarized as follows.

(1) Determine the structure of the BP neural network. The number of input layer nodes is $M = 3$, the number of hidden layer nodes is $Q = 5$, the number of output layer nodes is 3, and the initial values of the weighting coefficients of the hidden layer and the output layer are $\omega_{ij}^{(2)}(0)$ and $\omega_{li}^{(3)}(0)$, respectively. Determine the learning rate η and the inertia factor φ.

(2) The deviation of the rotor speed is calculated as $e(k) = r_{in}(k) - y_{out}(k)$.

(3) Normalize $r_{in}(k)$, $y_{out}(k)$, $y_{out}(k-1)$, $e(k)$, $e(k-1)$, $u(k)$, $u(k-1)$, and then select them as the input of the neural network.

(4) Calculate the input and output of the neurons in each layer of the neural network. Finally, the output layer outputs the three parameters Δk_p, Δk_i, and Δk_d required by the PID controller to determine the output $\Delta u(k)$ of the PID controller.

(5) According to the deviation between the expected value and the actual value, the weighting coefficients of the output layer and the hidden layer are corrected online by the neural network self-learning, and the PID controller parameters are adaptively adjusted until the deviation value reaches the ideal value.

(6) Set $k = k + 1$. Start a new cycle of parameter self-tuning to step(2) if the deviation value does not meet the requirements.

3) DESIGN OF BP-PID CONTROL ALGORITHM

a: FORWARD PROPAGATION

The input of the BP input layer is as follows.

$$O_j^{(1)}(k) = x(j) \quad (j = 1, 2, 3) \tag{22}$$

The input and output of the hidden layer are as follows [27].

$$net_i^{(2)}(k) = \sum_{j=1}^{3} \omega_{ij}^{(2)}(k) O_j^{(1)}(k) \quad (i = 1, 2, 3, 4, 5) \tag{23}$$

$$O_i^{(2)}(k) = f(net_i^{(2)}(k)) \tag{24}$$

where $\omega_{ij}^{(2)}(k)$ is the weight coefficient of the hidden layer, superscript (1) is the input layer, superscript (2) is the hidden layer.

The activation function of the hidden layer neurons is positive or negative, then the Sigmoid function of the hidden layer is as follows [29].

$$f(x) = \tanh(x) = \frac{e^x - e^{-x}}{e^x + e^{-x}} \tag{25}$$

The input and output of the output layer are as follows.

$$net_l^{(3)}(k) = \sum_{i=1}^{5} \omega_{li}^{(3)}(k) O_i^{(2)}(k) \quad (l = 1, 2, 3) \tag{26}$$

$$\begin{cases} O_l^{(3)}(k) = g(net_l^{(3)}(k)) \\ O_1^{(3)}(k) = \Delta k_p(k) \\ O_2^{(3)}(k) = \Delta k_i(k) \\ O_3^{(3)}(K) = \Delta k_d(k) \end{cases} \tag{27}$$

where $\omega_{li}^{(3)}(k)$ is the weight coefficient of the output layer, superscript (3) is the output layer. Since $\Delta k_p(k)$, $\Delta k_i(k)$, and $\Delta k_d(k)$ outputs of the BP neural network output layer are non-negative, the activation function of the output layer neurons is non-negative, then the Sigmoid function of the output layer is designed as follows.

$$g(x) = \frac{1}{2}(1 + \tanh(x)) = \frac{e^x}{e^x + e^{-x}} \tag{28}$$

b: BACK PROPAGATION

In order to reduce the deviation between the expected value and the actual sample value, the performance index function is selected as the criterion of the BP neural network correction weight coefficient [27], and the index function is expressed as follows.

$$E(k) = \frac{1}{2}(r_{in}(k) - y_{out}(k))^2 \tag{29}$$

According to the gradient descent method, the BP neural network weight is modified from the negative gradient direction, which uses $E(k)$ to adjusts the weight coefficient and keep the actual sample value at the expected value. Since the correction speed of the weight coefficient is slow and easy to enter a local optimum, it is necessary to increase the inertia term to compensate it [26]. The inertia term weight coefficient learning algorithm is as follows.

$$\begin{cases} \omega_{li}^{(3)}(k+1) = \omega_{li}^{(3)}(k) + \Delta\omega_{li}^{(3)}(k) \\ \Delta\omega_{li}^{(3)}(k) = -\eta \dfrac{\partial E(k)}{\partial \omega_{li}^{(3)}(k)} + \varphi \Delta\omega_{li}^{(3)}(k-1) \end{cases} \tag{30}$$

where

$$\frac{\partial E(k)}{\partial \omega_{li}^{(3)}(k)} = \frac{\partial E(k)}{\partial y(k)} \cdot \frac{\partial y(k)}{\partial \Delta u(k)} \cdot \frac{\partial \Delta u(k)}{\partial O_l^{(3)}(k)} \cdot \frac{\partial O_l^{(3)}(k)}{\partial net_l^{(3)}(k)} \cdot \frac{\partial net_l^{(3)}(k)}{\partial \omega_{li}^{(3)}(k)} \tag{31}$$

$$\frac{\partial net_l^{(3)}(k)}{\partial \omega_{li}^{(3)}(k)} = O_i^{(2)}(k) \tag{32}$$

Since the value of $\frac{\partial y(k)}{\partial \Delta u(k)}$ cannot be accurately calculated, the $sgn(\frac{\partial y(k)}{\partial \Delta u(k)})$ function is used to approximate it [28], and compensated for the learning efficiency η. According to the

TABLE 2. Parameters of BP-PID pitch controller.

Symbol	Parameter	Value
η	Learning rate	0.2
φ	Inertia coefficient	0.05
j	Number of cells in the input layer	3
i	Number of cells in the hidden layer	5
l	Number of cells in the output layer	3

above derivation, the formula (33) can be obtained.

$$\begin{cases} \dfrac{\partial \Delta u(k)}{\partial O_1^{(3)}(k)} = e(k) - e(k-1) \\ \dfrac{\partial \Delta u(k)}{\partial O_2^{(3)}(k)} = e(k) \\ \dfrac{\partial \Delta u(k)}{\partial O_3^{(3)}(k)} = e(k) - 2e(k-1) + e(k-2) \end{cases} \tag{33}$$

Through the above analysis, correction algorithm of the weight coefficient of the BP neural network output layer to the hidden layer is as follows.

$$\Delta\omega_{li}^{(3)}(k) = \varphi\Delta\omega_{li}^{(3)}(k-1) + \eta\delta_l^{(3)}(k)O_i^{(2)}(k) \tag{34}$$

$$\delta_l^{(3)}(k) = e(k) \cdot sgn\left(\frac{\partial y(k)}{\partial \Delta u(k)}\right) \cdot \frac{\partial \Delta u(k)}{\partial O_l^{(3)}(k)} \cdot g'(net_l^{(3)}(k)) \tag{35}$$

where

$$g'(x) = \frac{2}{e^x + e^{-x}} \tag{36}$$

In addition, according to the above derivation method, the weight coefficient correction algorithm of the BP neural network hidden layer to the input layer can be obtained as follows.

$$\Delta\omega_{ij}^{(2)}(k) = \varphi\Delta\omega_{ij}^{(2)}(k-1) + \eta\delta_i^{(2)}(k)O_j^{(1)}(k) \tag{37}$$

$$\delta_i^{(2)}(k) = f'(net_i^{(2)}(k)) \sum_{l=1}^{3} \delta_l^{(3)}(k)\omega_{li}^{(3)}(k) \tag{38}$$

where

$$f'(x) = \frac{4}{e^x + e^{-x}} \tag{39}$$

Through the above derivation, the weight coefficient learning algorithms for the hidden layer and the output layer are obtained, and three parameters of the PID controller can be adjusted in real time according to the deviation value.

The parameters of the BP-PID pitch controller are shown in TABLE 2.

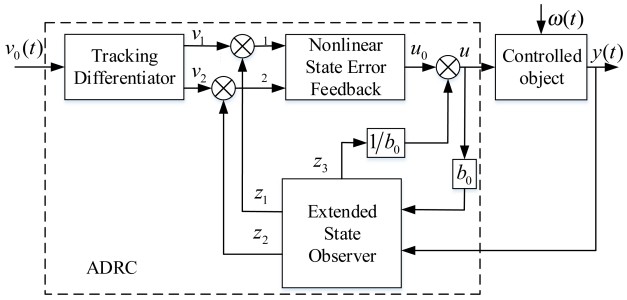

FIGURE 4. The structure diagram of ADRC.

B. DESIGN OF ACTIVE DISTURBANCE REJECTION PITCH CONTROLLER FOR WIND TURBINE

An active disturbance rejection controller is a nonlinear controller based on state observation and disturbance compensation, which has the function of disturbance estimation and compensation. It consists of three parts: Tracking Differentiator (TD), Extended State Observer (ESO) and Nonlinear State Error Feedback control law (NLSEF)[30]. Among them, TD is used for fast and no overshoot tracking of the system input signal, and gives the differential signal of the input signal, thus effectively solving the contradiction between rapidity and overshoot. ESO converts the nonlinear system into series integration type and estimates system state, unmodeled part and unknown disturbance. NLSEF configures nonlinear structure according to process error size and direction, which can improve the ability to suppress error signals.

Assuming that an nth-order nonlinear time-varying system is subject to unknown perturbations [32], it can be expressed as follows.

$$x^{(n)} = f(x, x^{(1)}, \cdots, x^{(n-1)}, t) + \omega(t) + bu(t) \tag{40}$$

where $f(x, x^{(1)}, \cdots, x^{(n-1)}, t)$ is an unknown function, $\omega(t)$ is the unknown disturbance of the system, x is the state variable, $u(t)$ is the control input, and b is the coefficient of the control input.

FIGURE 4. shows the structure of the second-order ADRC controller.

where $v_0(t)$ is a reference input, v_1 and v_2 are respectively a tracking signal and a differential signal of $v_0(t)$, z_1 is an estimated value of the output $y(t)$ of the controlled object, z_2 is an estimated value of the derivative of $y(t)$, z_3 is an estimated value of the total disturbance of the system.

According to formula (14), the wind turbine system can be expressed as a second-order system, and its active disturbance rejection control algorithm is designed as follows.

1) DESIGN OF TRACKING DIFFERENTIATOR

The input of the tracking differentiator is $v_0(k) = \omega_{ref}$, that is, the input is the reference value of rotor speed. By arranging a reasonable transition process, the generalized differential signal is extracted, and the overshoot caused by the excessive initial error is eliminated, thereby obtaining a smooth input signal. The differentiator of second-order nonlinear system is

as follows [33].

$$\begin{cases} \dot{v}_1(k) = v_2(k) \\ \dot{v}_2(k) = r^2 f(v_1(k) - v_0(k), \dfrac{v_2(k)}{r}) \end{cases} \tag{41}$$

where $v_1(k)$ is the tracking signal of $v_0(k)$, $v_2(k)$ is the differential signal of $v_0(k)$, r is the velocity factor.

As $v_1(k)$ can fully approach the input signal $v_0(k)$, formula (41) can be converted to formula (42).

$$\begin{cases} v_1(k+1) = v_1(k) + h \cdot v_2(k) \\ v_2(k+1) = v_2(k) + h \cdot fhan(v_1(k) \\ \qquad\qquad - v_0(k), v_2(k), r, h_0) \end{cases} \tag{42}$$

where h is the sampling period, h_0 is the filtering factor, usually the filtering factor h_0 is three to ten times that of the sampling period h, and $fhan(*)$ is a nonlinear function [34], whose expression is as follows.

$$fhan(v_1 - v_0, v_2, r, h_0) = \begin{cases} \dfrac{-r \cdot \alpha}{\delta} & |\alpha| \le \delta \\ -r \cdot sgn(\alpha) & |\alpha| > \delta \end{cases} \tag{43}$$

where

$$\alpha = \begin{cases} v_2 + \dfrac{y}{h_0} & |y| \le \delta_0 \\ v_2 + 0.5(\alpha_0 - \delta) \cdot sgn(y) & |y| > \delta_0 \end{cases} \tag{44}$$

$$\alpha_0 = \sqrt{\delta^2 + 8r\,|y|} \tag{45}$$

$$y = v_1 - v_0 + h \cdot v_2 \tag{46}$$

where $\delta = r \cdot h_0$, $\delta_0 = \delta \cdot h_0$, the range of α is $0 < \alpha < 1$, δ is the length of the interval of the linear segment. The velocity factor r needs to be determined according to the system conversion speed or the differential signal. The relationship between r and the conversion time t_0 is as follows.

$$r = \frac{4(v_1(k) - v_0(k))}{t_0^2} \tag{47}$$

The larger r is, the faster the conversion speed of the system is. The smaller r is, the more obvious the overshoot effect is suppressed. However, if r is too small, the response speed of the system is reduced and the transition time is increased. The parameters of the tracking differentiator are shown in TABLE 3.

The *sgn* function is a sign function, which can make full use of the maximum value of the control variable to quickly reach the control requirements, and is not sensitive to structural changes [36]. The expression is as follows.

$$sgn(y) = \begin{cases} 1 & y > 0 \\ 0 & y = 0 \\ -1 & y < 0 \end{cases} \tag{48}$$

2) DESIGN OF THE EXTENDED STATE OBSERVER

The extended state observer is the core part of the active disturbance rejection controller. It deduces the unmodeled parts and unknown disturbances of the system into the total disturbance of the system. In addition, the extended state observer real-time observes, evaluates, and compensates system state variables. An observer with one dimension larger than the system dimension is designed based on the nonlinear function $fhan(*)$. The combined effect of unmodeled parts and various disturbances is regarded as a new state-expansion state, which is observed by output feedback. In this paper, the wind turbine system is regarded as a second-order system, and the order of the extended state observer is designed as third-order. The designed observer expression is as follows.

TABLE 3. The parameters of TD.

Symbol	Parameter	Value
r	Tracking factor	50
h	The sampling period	0.001
h_0	Filter factor	0.005

$$\begin{cases} \varepsilon = z_1 - \omega_r \\ \dot{z}_1 = z_2 - \beta_1 fal(\varepsilon, \alpha_1, \delta_1) \\ \dot{z}_2 = z_3 - \beta_2 fal(\varepsilon, \alpha_2, \delta_1) + b_0 u(t) \\ \dot{z}_3 = -\beta_3 fal(\varepsilon, \alpha_3, \delta_1) \end{cases} \tag{49}$$

where ε is the deviation value, z_1 is the estimated value of the system state variable, that is, the estimated value of the rotor speed ω_r, z_2 is the estimated value of the derivative of the state variable, z_3 is the estimated value of the total disturbance of the system, β_1, β_2 and β_3 are coefficients of the nonlinear function, b_0 is the coefficient of the control input.

The role of the nonlinear function $fal(\varepsilon, \alpha, \delta)$ is to suppress signal chattering [37], which is expressed as follows.

$$fal(\varepsilon, \alpha, \delta) = \begin{cases} |\varepsilon|^\alpha \cdot sgn(\varepsilon) & |\varepsilon| > \delta_1 \\ \dfrac{\varepsilon}{\delta^{1-\alpha}} & |\varepsilon| \le \delta_1 \end{cases} \tag{50}$$

3) DESIGN OF NONLINEAR STATE ERROR FEEDBACK CONTROL LAW

According to the state deviation combined with the output of TD and ESO, the nonlinear structure is configured to form a nonlinear state error feedback control law. Its control law is designed as follows.

$$\begin{cases} \varepsilon_1(k) = v_1(k) - z_1(k) \\ \varepsilon_2(k) = v_2(k) - z_2(k) \\ u_0 = \beta_{01} fal(\varepsilon_1, \alpha_4, \delta_2) + \beta_{02} fal(\varepsilon_2, \alpha_5, \delta_2) \\ u_z = u_0 - z_3 / b_0 \end{cases} \tag{51}$$

where β_{01} and β_{02} are coefficients of the non-linear function.

4) DESIGN OF DISTURBANCE REJECTION VARIABLE PITCH CONTROLLER

In the process of linearizing the wind turbine model, when the output power of the wind power system is stable, a stable point A is selected, and the coordinate values of the point are T_{w0}, θ_0, and ω_0. θ_0 and ω_0 are the pitch angle and the rotational speed of the wind turbine at the equilibrium point, respectively. T_{w0} is the mechanical torque generated

by the wheel at the equilibrium point. At point A, the Taylor expansion of the function $T_w(\omega, \theta, V)$ is expressed as follows.

$$\begin{aligned} T_w - T_{w0} &= \frac{\partial T_w}{\partial \omega}\Delta\omega + \frac{\partial T_w}{\partial \theta}\Delta\theta + \frac{\partial T_w}{\partial V}\Delta V + \Delta h \\ &= \mu\Delta\omega + \xi\Delta\theta + \gamma\Delta V + \Delta h \end{aligned} \tag{52}$$

where Δh is the expansion high-order term, $\mu = \frac{\partial T_w}{\partial \omega}$, $\xi = \frac{\partial T_w}{\partial \theta}$ and $\gamma = \frac{\partial T_w}{\partial V}$.

When the wind speed is above the rated wind speed, T_{w0} can be expressed as follows.

$$T_{w0} = T_D + \gamma T_e \tag{53}$$

The dynamic characteristic expression of the variable pitch actuator of the wind turbine system is as follows.

$$\theta - \theta_0 = \Delta\theta = \frac{1}{\tau s + 1}\Delta\theta_r \tag{54}$$

Let $J = J_w + \gamma^2 J_g$, take $\Delta\omega$ as the controller input, and combine with formula (13) to derive its first and second order differential equations as follows.

$$\begin{aligned} J\Delta\dot{\omega} &= J\dot{\omega} - J\dot{\omega}_0 \\ &= T_{w0} + \mu\Delta\omega + \xi\Delta\theta + \gamma\Delta V + \Delta h - T_e \end{aligned} \tag{55}$$

$$\begin{aligned} J\Delta\ddot{\omega} &= J\ddot{\omega} - J\ddot{\omega}_0 \\ &= \frac{\tau\mu - J}{\tau}\Delta\dot{\omega} + \frac{\mu}{\tau}\Delta\omega + \frac{\xi}{\tau}\Delta\theta_r \\ &\quad + \frac{\tau s + 1}{\tau}(\gamma\Delta V + \Delta h) \end{aligned} \tag{56}$$

The coefficient corresponding to the $\Delta\theta_r$ term is easy to change as the system is running, and it is difficult to obtain the exact value. Therefore, the estimated value b_0 is used to replace it, and the error of the estimation is classified as the internal disturbance of the system.

Then formula (56) can be converted into formula (57) as follows.

$$\Delta\ddot{\omega} = \frac{\tau\mu - J}{J\tau}\Delta\dot{\omega} + \frac{\mu}{J\tau}\Delta\omega + b_0\Delta\theta_r + d \tag{57}$$

where $\Delta\omega = \omega_r - \omega_0$ is the input of the extended state observer. $\Delta\theta_r$, the pitch angle that the pitch system needs to adjust, is the output of the active disturbance rejection controller.

According to formula (2) and formula (52), b_0 is taken as follows.

$$b_0 = \frac{1}{J\tau} \cdot \frac{\partial T_w}{\partial \theta} \tag{58}$$

The system disturbance amount d can be expressed as follows.

$$d = \frac{\tau s + 1}{J\tau}(\gamma\Delta V + \Delta h) + (\frac{\xi}{J\tau} - b_0)\Delta\theta_r \tag{59}$$

The design of the ADRC pitch controller is shown in formula (60).

$$\begin{cases} \varepsilon = \Delta\omega = z_1 - \omega_0 \\ u_z(k) = \Delta\theta_r = -\dfrac{z_3}{b_0} + \beta_{01} fal(\varepsilon, \alpha_4, \delta_2) \\ \qquad + \beta_{02} fal(\varepsilon, \alpha_5, \delta_2) \end{cases} \tag{60}$$

TABLE 4. The parameters of active disturbance rejection controller.

Symbol	Parameter	Value
α_1	Adjustable parameter	0.5
α_2	Adjustable parameter	0.25
α_3	Adjustable parameter	0.3
α_4	Adjustable parameter	0.75
α_5	Adjustable parameter	1.5
δ_1	The length of the interval of the linear segment	0.0025
δ_2	The length of the interval of the linear segment	0.02
β_1	The coefficient of the nonlinear function	100
β_2	The coefficient of the nonlinear function	300
β_3	The coefficient of the nonlinear function	1000
β_{01}	The coefficient of the nonlinear function	6.0
β_{02}	The coefficient of the nonlinear function	1.5

Finally, combined with BP-PID controller and active disturbance rejection controller, according to formulas (18) and (60), the final pitch control law is as follows.

$$u = \theta_r = u(k) + u_z(k) \tag{61}$$

The parameters of active disturbance rejection controller are shown in TABLE 4.

5) STABILITY VERIFICATION

Transform formula (16) into a single input single output affine nonlinear system as follows.

$$\begin{cases} \dot{x} = \mathbb{R}(x) + \mathbb{Q}(x)u \\ y = C(x) = P_e(x) \end{cases} \tag{62}$$

where u is the input control variable, y is the output variable, $\mathbf{x} = [x_1, x_2, \cdots, x_n]^T$ is the n-order state vector. then

$$\begin{aligned} \mathbb{R}(x) &= \begin{bmatrix} \mathbb{R}_1(x) \\ \mathbb{R}_2(x) \end{bmatrix} \\ &= \begin{bmatrix} -\dfrac{1}{T_\theta}x_1 + F_1(x_1, x_2, \omega(t)) \\ \dfrac{1}{J_w + \gamma^2 J_g}[T_w - T_D - \gamma T_{em}] + F_2(x_1, x_2, \omega(t)) \end{bmatrix} \end{aligned} \tag{63}$$

$$\mathbb{Q}(x) = \begin{bmatrix} \mathbb{Q}_1(x) \\ \mathbb{Q}_2(x) \end{bmatrix} = \begin{bmatrix} \dfrac{1}{T_\theta} \\ 0 \end{bmatrix} \tag{64}$$

$$\begin{aligned} &F(x, \omega(t)) \\ &\quad = F_1(x_1, x_2, \omega(t)) + F_2(x_1, x_2, \omega(t)) \end{aligned} \tag{65}$$

where $F_1(x_1, x_2, \omega(t))$ and $F_2(x_1, x_2, \omega(t))$ are the disturbance function of the wind turbine system, $\omega(t)$ is the external

disturbance, $F(x, \omega(t))$ is the total disturbances of the system, Let $\dot{F}(x, \omega(t)) = H$, then formula (62) can be expressed as follows.

$$\begin{cases} \dot{x}_1 = x_2 \\ \dot{x}_2 = x_3 + b_0 u \\ \dot{x}_3 = \dot{F}(x, \omega(t)) = H(x_1, x_2, \omega(t)) \\ \tilde{y} = x_1 \end{cases} \tag{66}$$

where $X = [x_1, x_2, x_3]^T = \left[\theta, \dot{\theta}, F(x, \omega(t))\right]^T$, b_0 is a constant. According to the extended state observer in formula (49), we know that $Z = [z_1, z_2, z_3]^T$ is the estimated value of X. Let the controlled object in formula (62) track the bounded input Γ, combine the output of the extended state observer and the nonlinear state error feedback control law to make the following feedback control.

$$u = \frac{\kappa_1}{b_0}(\Gamma - x_1) + \frac{\kappa_2}{b_0}(\dot{\Gamma} - x_2) + \frac{1}{b_0}(\ddot{\Gamma} - x_3) \tag{67}$$

where κ_1 and κ_2 are the parameters of controller.

Let $\Gamma_1 = \Gamma, \Gamma_2 = \dot{\Gamma}, \Gamma_3 = \ddot{\Gamma}$. As $\Gamma = \omega_{ref}$ is a constant, we can obtain $\Gamma_2 = \Gamma_3 = 0$. Let $E_i = \Gamma_i - x_i (i = 1, 2)$, $\varepsilon_j = x_j - z_j (j = 1, 2, 3)$. According to formulas (49) and (51), the output error of the system and the observation error of the extended state observer can be obtained as follows.

$$\begin{cases} \dot{E}_1 = \dot{\Gamma}_1 - \dot{x}_1 = \Gamma_2 - x_2 = E_2 \\ \dot{E}_2 = \dot{\Gamma}_2 - \dot{x}_2 = \Gamma_3 - x_3 - b_0 u \\ = -\varepsilon_3 - \kappa_1(E_1 + \varepsilon_1) - \kappa_2(E_2 + \varepsilon_2) \\ \dot{\varepsilon}_1 = \varepsilon_2 - \beta_1 \varepsilon_1 \\ \dot{\varepsilon}_2 = \varepsilon_3 - \beta_2 \varepsilon_1 \\ \dot{\varepsilon}_3 = H(x_1, x_2, \omega(t)) - H(z_1, z_2, \omega(t)) - \beta_3 \varepsilon_1 \end{cases} \tag{68}$$

Let $H(x_1, x_2, \omega(t)) - H(z_1, z_2, \omega(t)) = G_1$. We can obtain $G_1 = 0$ when $\varepsilon_1 = \varepsilon_2 = 0$. Therefore, $D = \begin{bmatrix} 0 & 0 & 0 & 0 & 0 \end{bmatrix}$ is the equilibrium of the system in formula (68). The parameters of the controller can be designed as $\begin{bmatrix} \beta_1 & \beta_2 & \beta_3 \end{bmatrix} = \begin{bmatrix} 3\chi_1 & 3\chi_1^2 & \chi_1^3 \end{bmatrix}$ and $\begin{bmatrix} \kappa_1 & \kappa_2 \end{bmatrix} = \begin{bmatrix} \chi_2^2 & 2\chi_2 \end{bmatrix}$. Then, formula (68) can be expressed by the following matrix.

$$\dot{E} = AE + BG_1 \tag{69}$$

where

$$E = \begin{bmatrix} E_1 & E_2 & \varepsilon_1 & \varepsilon_2 & \varepsilon_3 \end{bmatrix}^T,$$

$$A = \begin{bmatrix} 0 & 1 & 0 & 0 & 0 \\ -\chi_2^2 & -2\chi_2 & -\chi_2^2 & -2\chi_2 & -1 \\ 0 & 0 & -3\chi_1 & 1 & 0 \\ 0 & 0 & -3\chi_1^2 & 0 & 1 \\ 0 & 0 & -\chi_1^3 & 0 & 0 \end{bmatrix},$$

$$B = \begin{bmatrix} 0 & 0 & 0 & 0 & 1 \end{bmatrix}^T.$$

The eigenvalues of matrix A is as follows.

$$\left|\tilde{\lambda} I - A\right| = (\tilde{\lambda} + \chi_2)^2 (\tilde{\lambda} + \chi_1)^3 \tag{70}$$

We can obtain $\tilde{\lambda}_1 = \tilde{\lambda}_2 = -\chi_2, \tilde{\lambda}_3 = \tilde{\lambda}_4 = \tilde{\lambda}_5 = -\chi_1$.

Then

$$J = \begin{bmatrix} -\chi_2 & 1 & 0 & 0 & 0 \\ 0 & -\chi_2 & 1 & 0 & 0 \\ 0 & 0 & -\chi_1 & 1 & 0 \\ 0 & 0 & 0 & -\chi_1 & 1 \\ 0 & 0 & 0 & 0 & -\chi_1 \end{bmatrix} \tag{71}$$

The eigenvectors of matrix A are calculated as follows.

$$P = \begin{bmatrix} 1 & 0 & 1 & 2 & 3 \\ -\chi_2 & 1 & 4 & 5 & 6 \\ 0 & 0 & \frac{1}{\chi_1^2} & -\frac{1}{\chi_1^3} & 0 \\ 0 & 0 & \frac{2}{\chi_1} & -\frac{1}{\chi_1^2} & -\frac{1}{\chi_1^3} \\ 0 & 0 & 1 & 0 & 0 \end{bmatrix} \tag{72}$$

where

$$\upsilon_1 = -\frac{\chi_2^2 + \chi_1^2 + 4\chi_1\chi_2}{\chi_1^2(\chi_2 - \chi_1)^2}, \quad \upsilon_2 = \frac{\chi_2^2 + \chi_1^2 + 4\chi_1\chi_2}{\chi_1(\chi_2 - \chi_1)^2},$$

$$\upsilon_3 = \frac{\chi_2^3 + 3\chi_2^2\chi_1 + 6\chi_2\chi_1^2 + 2\chi_1^3}{\chi_1^3(\chi_2 - \chi_1)^3}$$

$$\upsilon_4 = -\frac{2\chi_2^3 + 6\chi_2^2\chi_1 + 3\chi_2\chi_1^2 + \chi_1^3}{\chi_1^2(\chi_2 - \chi_1)^3}$$

$$\upsilon_5 = -\frac{9\chi_2^2 + 6\chi_2\chi_1 + 3\chi_1^2}{\chi_1^2(\chi_2 - \chi_1)^4}$$

$$\upsilon_6 = \frac{\chi_2^4 + 2\chi_2^3\chi_1 + 12\chi_2^2\chi_1^2 + 2\chi_2\chi_1^3 + \chi_1^4}{\chi_1^3(\chi_2 - \chi_1)^4}.$$

The inverse of matrix P is as follows.

$$P^{-1} = \begin{bmatrix} * & * & * & * & \frac{6\chi_1^2 + 12\chi_2\chi_1}{(\chi_2 - \chi_1)^4} \\ * & * & * & * & \frac{3\chi_1^2 + 3\chi_2\chi_1}{(\chi_2 - \chi_1)^3} \\ * & * & * & * & 1 \\ * & * & * & * & \chi_1 \\ * & * & * & * & \chi_1^2 \end{bmatrix} \tag{73}$$

Since only the last column of the inverse matrix P^{-1} is needed for subsequent calculations, no other terms of the inverse matrix are given here.

Define a matrix as

$$M = \begin{bmatrix} \hbar_1 & \hbar_2 & \hbar_3 & \hbar_4 & \hbar_5 \end{bmatrix}^T \tag{74}$$

Transform matrix $E = PM$, then $G_1 \leq L_h \|P_0 M\|$.
where L_h is the Lipschitz constant,

$$P_0 = \begin{bmatrix} 0 & 0 & \frac{1}{\chi_1^2} & -\frac{1}{\chi_1^3} & 0 \\ 0 & 0 & \frac{2}{\chi_1} & -\frac{1}{\chi_1^2} & -\frac{1}{\chi_1^3} \end{bmatrix}.$$

Then

$$\dot{M} = JM + P^{-1}BG_1 \tag{75}$$

where

$$P^{-1}B = \begin{bmatrix} \frac{6\chi_1^2 + 12\chi_2\chi_1}{(\chi_2-\chi_1)^4} \\ \frac{3\chi_1^2 + 3\chi_2\chi_1}{(\chi_2-\chi_1)^3} \\ 1 \\ \chi_1 \\ \chi_1^2 \end{bmatrix},$$

$$\dot{\hbar}_1 = -\chi_2\hbar_1 + \hbar_2 + \frac{6\chi_1^2 + 12\chi_2\chi_1}{(\chi_2-\chi_1)^4}G_1,$$
$$\dot{\hbar}_2 = -\chi_2\hbar_2 + \frac{3\chi_1^2 + 3\chi_2\chi_1}{(\chi_2-\chi_1)^3}G_1,$$
$$\dot{\hbar}_3 = -\chi_1\hbar_3 + \hbar_4 + G_1, \quad \dot{\hbar}_4 = -\chi_1\hbar_4 + \hbar_5 + \chi_1 G_1,$$
$$\dot{\hbar}_5 = -\chi_1\hbar_5 + \chi_1^2 G_1.$$

According to the above inference, a Lyapunov function can be constructed as follows.

$$\begin{aligned} V_{ly} = {} & \frac{1}{2}(2\chi_2\hbar_1 + \hbar_2)^2 + (\frac{1}{2} + 2\chi_2^2)\hbar_2^2 \\ & + \frac{\chi_2}{2\chi_1}(2\chi_2\hbar_3 + \frac{\chi_2}{\chi_1}\hbar_4 + \frac{\chi_2}{2\chi_1^2}\hbar_5)^2 \\ & + \frac{1}{2}(\sqrt{\frac{\chi_2^3(1+4\chi_1^2)}{\chi_1^3}}\hbar_4 \\ & + \frac{(1+2\chi_1^2)\sqrt{\chi_2^3\chi_1(1+4\chi_1^2)}}{\chi_1^3(1+4\chi_1^2)}\hbar_5)^2 \\ & + \frac{1}{2}(\frac{\chi_2^3}{4\chi_1^5} + \frac{4\chi_2^3}{\chi_1} + \frac{2\chi_2^3(1+2\chi_1^2)}{(1+4\chi_1^2)\chi_1^3})\hbar_5^2 \end{aligned} \tag{76}$$

Then

$$\begin{aligned} \dot{V}_{ly} = {} & -4\chi_2^3[(\hbar_1^2 + \hbar_2^2 + \hbar_3^2 + \hbar_4^2 + \hbar_5^2) \\ & - \frac{12\chi_1^2\chi_2 + 27\chi_1\chi_2^2 - 3\chi_1^3}{2\chi_2^2(\chi_2-\chi_1)^4}G_1\hbar_1 \\ & - \frac{6\chi_1^2\chi_2 + 15\chi_2^2\chi_1 + 6\chi_1\chi_2^4 - 3\chi_1^3 - 6\chi_1^3\chi_2^2}{2\chi_2^3(\chi_2-\chi_1)^4}G_1\hbar_2 \\ & - \frac{7}{4\chi_1}G_1\hbar_3 - \frac{11+12\chi_1^2}{8\chi_1^2}G_1\hbar_4 \\ & - (\frac{1+5\chi_1^2+5\chi_1^4+4\chi_1^6}{\chi_1^3(1+4\chi_1^2)})G_1\hbar_5] \end{aligned} \tag{77}$$

According to Cauchy inequality $(\sum_{i=1}^{n} a_i^2)(\sum_{i=1}^{n} b_i^2) \geq (\sum_{i=1}^{n} a_i b_i)^2$, the following formula (78) can be obtained.

$$\begin{aligned} & \frac{12\chi_1^2\chi_2 + 27\chi_1\chi_2^2 - 3\chi_1^3}{2\chi_2^2(\chi_2-\chi_1)^4}G_1\hbar_1 \\ & + \frac{6\chi_1^2\chi_2 + 15\chi_2^2\chi_1 + 6\chi_1\chi_2^4 - 3\chi_1^3 - 6\chi_1^3\chi_2^2}{2\chi_2^3(\chi_2-\chi_1)^4}G_1\hbar_2 \\ & + \frac{7}{4\chi_1}G_1\hbar_3 + \frac{11+12\chi_1^2}{8\chi_1^2}G_1\hbar_4 \\ & + (\frac{1+5\chi_1^2+5\chi_1^4+4\chi_1^6}{\chi_1^3(1+4\chi_1^2)})G_1\hbar_5 \leq \lambda\sqrt{G_1^2M^2} \\ & \leq L_h\lambda\|P_0\|M^2 \end{aligned} \tag{78}$$

where

$$\lambda = \sqrt{\ell_1^2 + \ell_2^2 + \ell_3^2 + \ell_4^2 + \ell_5^2},$$
$$\ell_1 = \frac{12\chi_1^2\chi_2 + 27\chi_2^2\chi_1 - 3\chi_1^3}{2\chi_2^2(\chi_2-\chi_1)^4},$$
$$\ell_2 = \frac{6\chi_1^2\chi_2 + 15\chi_2^2\chi_1 + 6\chi_2^4\chi_1 - 3\chi_1^3 - 6\chi_1^3\chi_2^2}{2\chi_2^3(\chi_2-\chi_1)^4},$$
$$\ell_3 = \frac{7}{4\chi_1}, \quad \ell_4 = \frac{11+12\chi_1^2}{8\chi_1^2},$$
$$\ell_5 = \frac{1+5\chi_1^2+5\chi_1^4+4\chi_1^6}{\chi_1^3(1+4\chi_1^2)}.$$

Then

$$\dot{V} \leq -4\chi_2^3(1 - L_h\lambda\|P_0\|)M^2 \tag{79}$$

It is easy to see that V is positive definite, and when formula (80) is established, $\dot{V}$ is negative definite.

$$L_h\lambda\|P_0\| < 1 \tag{80}$$

Therefore, according to the Lyapunov theorem, the closed-loop system of in formula (75) is stable, which is $\lim_{t\to\infty} M(t) = 0$. Then, $\lim_{t\to\infty} PM(t) = 0$ and $\lim_{t\to\infty} E(t) = 0$. So give any initial value, it will meet $\lim_{t\to\infty} \tilde{y}_i = \Gamma_i (i = 1, 2)$ and $\lim_{t\to\infty} x_j = z_j (j = 1, 2, 3)$. So the extended state observer can well track the system input and estimate the system state, making the system output converge. For a given wind speed V and rotor speed ω_{ref}, the extended state observer is stable.

In addition, we also adopt continuous step wind speed to verify the stability of the compound controller.

IV. SIMULATION RESULTS AND ANALYSIS

A 3MW wind turbine pitch control system was simulated by MATLAB/Simulink software to verify the effectiveness of the proposed control algorithm. The research in this paper is mainly for the area above the rated wind speed, whose goal is to minimize the fluctuation of the rotor speed and keep the output power at the rated value. The simulation experiment of wind turbine pitch control is carried out in step wind speed and random wind speed, respectively. The step wind speed is shown in FIGURE 5. (a), and the random wind speed is shown in FIGURE 9. (a).

A. STEP WIND SPEED TEST

The ESO in the active disturbance rejection controller can observe and estimate system state variables, derivatives of state variables, and total system disturbances. It can be known

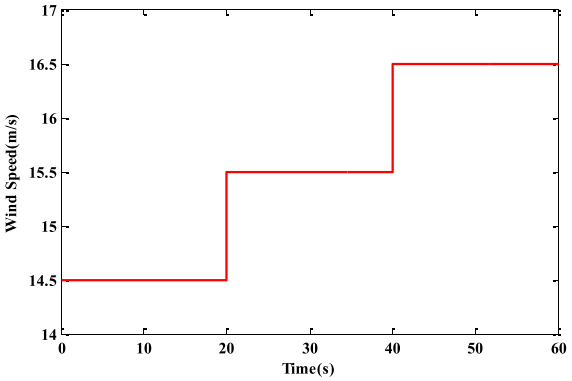

(a) Step wind speed

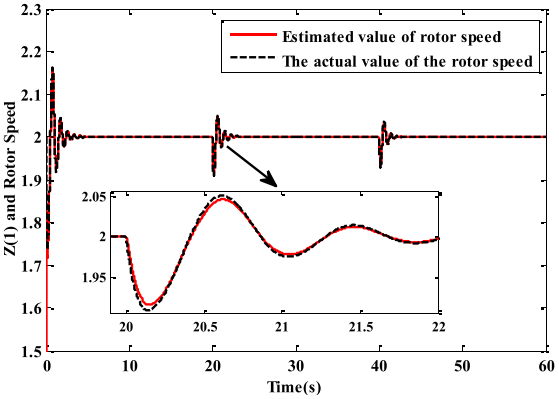

(b) The actual value and estimated value of rotor speed

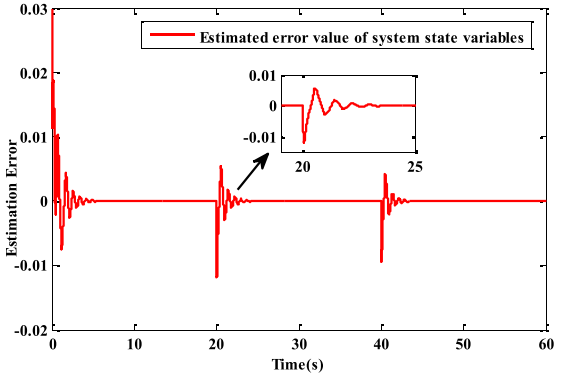

(c) The estimated error of ESO on rotor speed

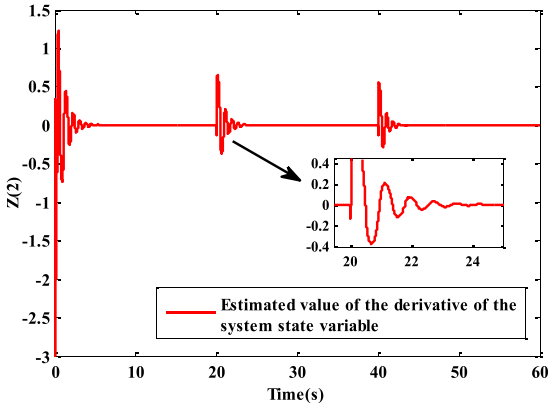

(d) The estimated value of the derivative of system state variable

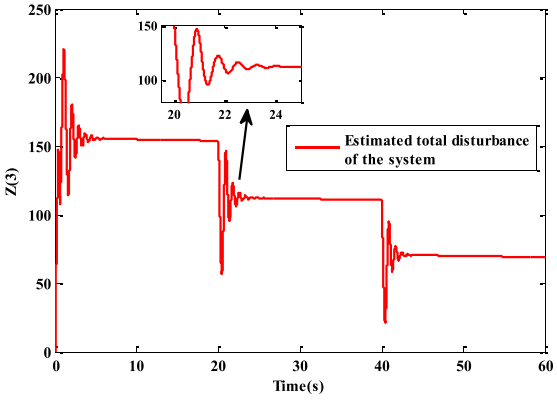

(e) The estimated total disturbances of the system

FIGURE 5. (a) Step wind speed; (b) The actual value and estimated value of rotor speed; (c) The estimated error of ESO on rotor speed; (d) The estimated value of the derivative of system state variable; (e) The estimated total disturbances of the system.

from formula (49) that z_1 is an estimated value of the state variable rotor speed for the ESO, which is an estimated value of the rotor speed, z_2 is an estimated value of the derivative of the state variable, z_3 is an estimated value of the total disturbance for the system, ε is the value of the estimated error of the system state variable. FIGURE 5. (b) is a comparison between the actual rotor speed of the wind turbine and the estimated rotor speed in the ESO. FIGURE 5. (c) is the deviation of the rotor speed estimated by the ESO. FIGURE 5. (d) is the estimated value of the derivative of the system state variable. FIGURE 5. (e) is the total disturbances of the system estimated by the ESO.

To verify the response speed, overshoot and dynamic performance of the system in the step wind speed shown in FIGURE 5. (a), the wind turbine pitch angle variation curve, rotor speed variation curve and output power variation curve are obtained, respectively. From FIGURE 6. (a) to FIGURE 6. (c) that compared with the PID and BP-PID pitch control algorithms, we can know that the ADRC-BP-PID pitch control algorithm proposed in this paper can make the rotor speed

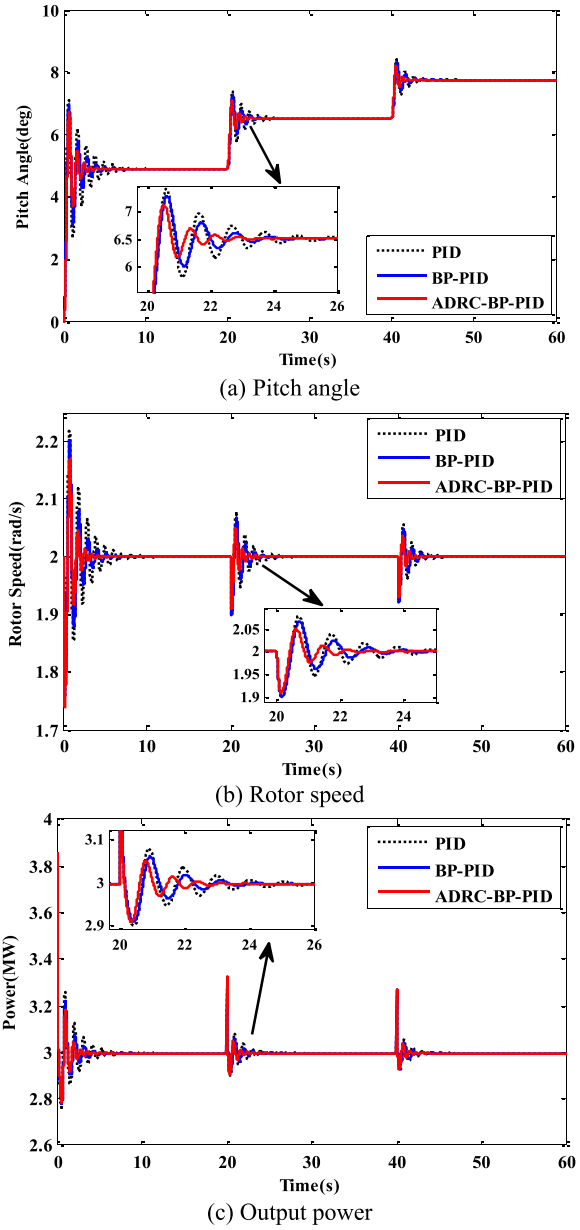

FIGURE 6. (a) Pitch angle; (b) Rotor speed; (c) Output power.

and output power have the smallest fluctuation range, fastest stability, strongest anti-interference ability, and best dynamic performance.

Under the condition of the step wind speed shown in FIGURE 5. (a), the rotor speed total fluctuations contrast diagram and the output power total fluctuations contrast diagram among the PID, BP-PID and ADRC-BP-PID controllers can be obtained, as respectively shown in FIGURE 7. and FIGURE 8. FIGURE 7. shows the total fluctuations of rotor speed in periods 0 to 8 seconds, 20 to 28 seconds, 40 to 48 seconds, respectively. FIGURE 8. shows the total fluctuations of output power in periods 0 to 8 seconds, 20 to 28 seconds, 40 to 48 seconds, respectively. It can be seen from FIGURE 7. that the ADRC-BP-PID pitch controller can reduce the fluctuations of the rotor speed under the conditions of the wind speed of 14.5m/s, 15.5m/s, and 16.5m/s. And as shown in FIGURE 8., the proposed ADRC-BP-PID pitch controller can reduce the output power fluctuations. Therefore, the ADRC-BP-PID controller has the best control performance.

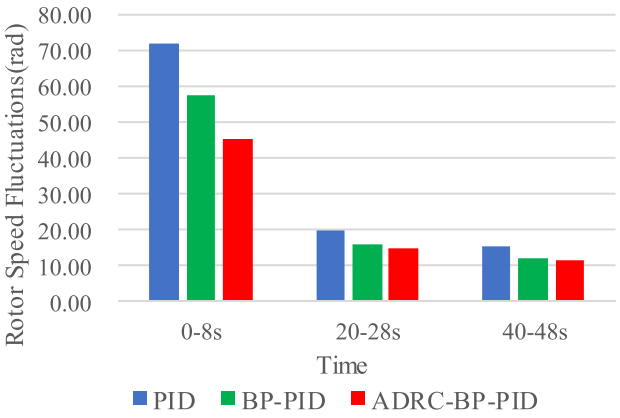

FIGURE 7. The total fluctuations comparison of rotor speed in three different periods.

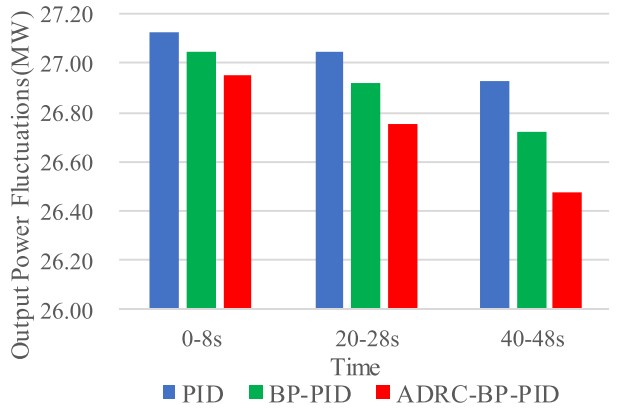

FIGURE 8. The total fluctuations comparison of output power in three different periods.

B. RANDOM WIND SPEED TEST

Under the condition of the random wind speed shown in FIGURE 9. (a), the comparison between the actual rotor speed of the wind turbine and the estimated value of the rotor speed in the ESO can be obtained from FIGURE 9. (b). FIGURE 9. (c) is the deviation of the rotor speed estimated by the ESO. FIGURE 9. (d) is the estimated value of the derivative of the system state variable. FIGURE 9. (e) is the total disturbances of the system estimated by the ESO.

FIGURE 10. (a) to FIGURE 10. (c) are the pitch angle variation curve, the rotor speed variation curve and the output power variation curve under random wind speed condition, respectively. It can be known from FIGURE 10. (a), FIGURE 10. (b) and FIGURE 10. (c) that the ADRC-BP-PID pitch control algorithm has the smallest overshoot and best stability in the three different pitch control algorithms. In addition,

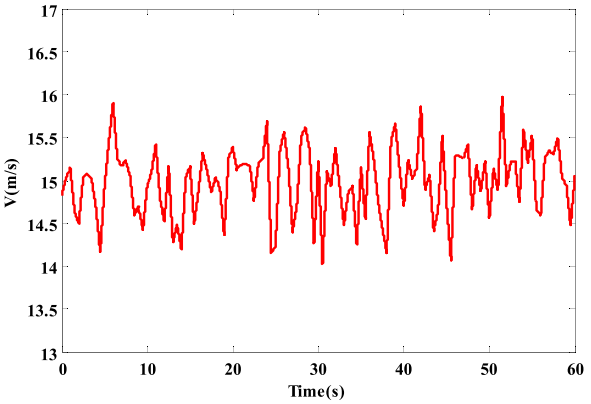

(a) Random wind speed

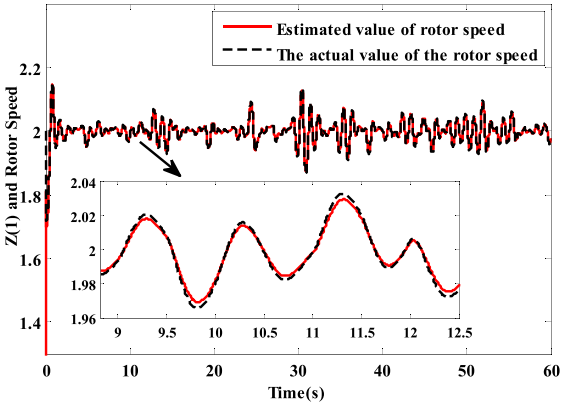

(b) The actual value and estimated value of rotor speed

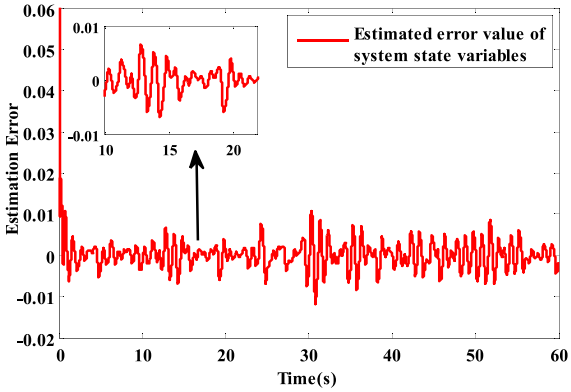

(c) The estimated error of ESO on rotor speed

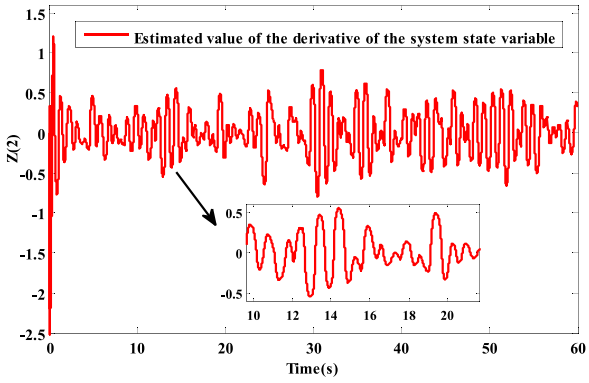

(d) The estimated value of the derivative of system state variable

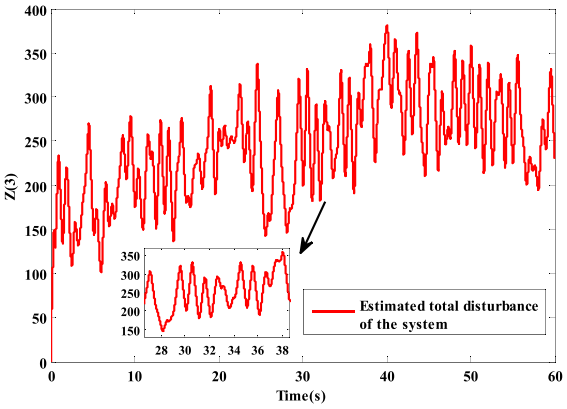

(e) The estimated total disturbances of the system

FIGURE 9. (a) Random wind speed; (b) The actual value and estimated value of rotor speed; (c) The estimated error of ESO on rotor speed; (d) The estimated value of the derivative of system state variable; (e) The estimated total disturbances of the system.

the amplitude of the pitch angle changing is the smallest, which effectively reduces the fatigue of the pitch actuator and the mechanical abrasion between the components. Simultaneously, the wind turbine can extend its service life and reduce its failure rate. As the amplitude of the pitch angle changing of the ADRC-BP-PID controller is the smallest, it has the smallest impact on the rotor speed and output power characteristics of the system. It can be seen from FIGURE 10. (b) and FIGURE 10. (c) that compared with the PID and BP-PID pitch control algorithms, the ADRC-BP-PID pitch control algorithm has the smallest fluctuations of rotor speed and output power, which has ideal effect on the amplitude suppression of the speed and power. The smooth pitching action reduces the amplitude changing of the output power, and keeps the speed of the rotor at the rated speed, which effectively improves the performance of the variable pitch system of the wind turbine.

Under the action of the random wind speed shown in FIGURE 9.(a), the rotor speed and output power total fluctuations contrast diagram among the PID, BP-PID and

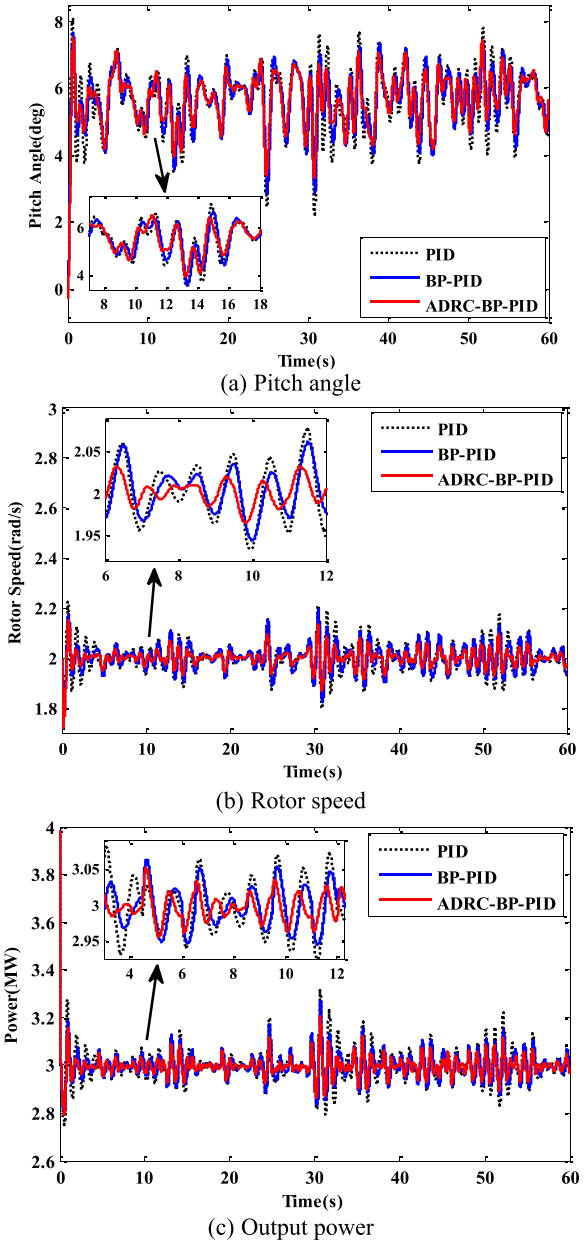

FIGURE 10. (a) Pitch angle; (b) Rotor speed; (c) Output power.

ADRC-BP-PID controllers can be obtained, as shown in FIGURE 11., in which the unit of rotor speed is rad/s, and the unit of output power is MW. And the figure shows the total fluctuations of rotor speed and output power from 0 to 60 seconds, respectively. It can be seen from FIGURE 11. that the ADRC-BP-PID pitch controller can effectively adjust the rotor speed, reduce the output power fluctuation, which enhances the stability of the wind turbine system.

V. CONCLUSION

In the feedback control loop, BP-PID pitch controller corrects the weights of its output layer and hidden layer by BP neural network self-learning according to the deviation of

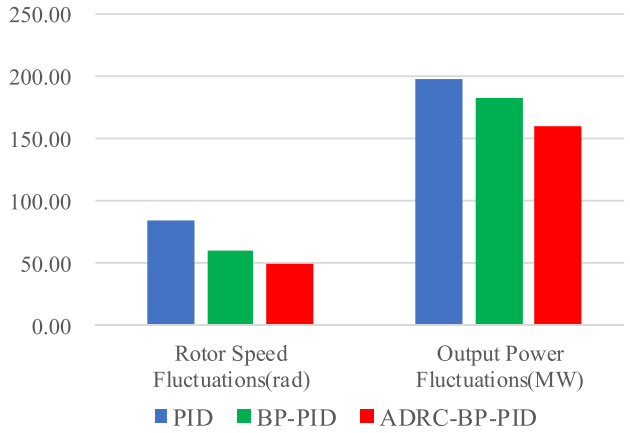

FIGURE 11. The total fluctuations of rotor speed and output power under random wind.

the rotor speed. Thereby, the PID parameters are adjusted online, and the problem of optimizing the PID parameters is solved. In addition, for the various uncertain disturbances and mechanical component parameter changing in the actual wind farm, an active disturbance rejection controller is designed to compensate the BP-PID pitch controller. The active disturbance controller can effectively estimate and compensate the system state variables and system disturbances. According to the state error, the ADRC can configure the nonlinear structure to replace the linear weight sum in the PID control and further form a nonlinear state error feedback control law to realize the compensation for the BP-PID pitch controller. The pitch control algorithm proposed in this paper can reduce the amplitude of the pitch angle changing and improve the response speed. Therefore, the performance of the wind turbine pitch control system is improved.

REFERENCES

[1] G. Noshirvani, J. Askari, and A. Fekih, "A robust fault detection and isolation filter for the pitch system of a variable speed wind turbine," *Int. Trans. Electr. Energy Syst.*, vol. 28, no. 11, Nov. 2018, Art. no. e2625.

[2] S. Soued, M. A. Ebrahim, H. S. Ramadan, and M. Becherif, "Optimal blade pitch control for enhancing the dynamic performance of wind power plants via Metaheuristic optimisers," *IET Electr. Power Appl.*, vol. 11, no. 8, pp. 1432–1440, Sep. 2017.

[3] Z. Zhao, S. Qian, W. Shen, T. Wang, B. Xu, Y. Zheng, and R. Wang, "Study on variable pitch strategy in H-type wind turbine considering effect of small angle of attack," *J. Renew. Sustain. Energy*, vol. 9, no. 5, Sep. 2017, Art. no. 053302.

[4] M. Ansari, M. R. H. Nobari, and E. Amani, "Determination of pitch angles and wind speeds ranges to improve wind turbine performance when using blade tip plates," *Renew. Energy*, vol. 140, pp. 957–969, Sep. 2019.

[5] H. Habibi, I. Howard, and S. Simani, "Reliability improvement of wind turbine power generation using model-based fault detection and fault tolerant control: A review," *Renew. Energy*, vol. 135, no. 5, pp. 877–896, May 2019.

[6] H. Jafarnejadsani, J. Pieper, and J. Ehlers, "Adaptive control of a variable-speed variable-pitch wind turbine using radial-basis function neural network," *IEEE Trans. Control Syst. Technol.*, vol. 21, no. 6, pp. 2264–2272, Nov. 2013.

[7] X. Tong and X. Zhao, "Power generation control of a monopile hydrostatic wind turbine using an H_∞ loop-shaping torque controller and an LPV pitch controller," *IEEE Trans. Control Syst. Technol.*, vol. 26, no. 6, pp. 2165–2172, Nov. 2018.

[8] M.-W. Ge, W.-M. Ke, and H.-X. Chen, "Pitch control strategy before the rated power for variable speed wind turbines at high altitudes," *J. Hydrodynamics*, vol. 31, no. 2, pp. 379–388, Apr. 2019.
[9] M. Rahimi and M. Asadi, "Control and dynamic response analysis of full converter wind turbines with squirrel cage induction generators considering pitch control and drive train dynamics," *Int. J. Electr. Power Energy Syst.*, vol. 108, pp. 280–292, Jun. 2019.
[10] H. Habibi, H. R. Nohooji, I. Howard, and S. Simani, "Fault-tolerant neuro adaptive constrained control of wind turbines for power regulation with uncertain wind speed variation," *Energies*, vol. 12, no. 24, p. 4712, Dec. 2019.
[11] Y. Ren, L. Li, J. Brindley, and L. Jiang, "Nonlinear PI control for variable pitch wind turbine," *Control Eng. Pract.*, vol. 50, pp. 84–94, May 2016.
[12] H. Ren, H. Zhang, G. Deng, and B. Hou, "Feedforward feedback pitch control for wind turbine based on feedback linearization with sliding mode and fuzzy PID algorithm," *Math. Problems Eng.*, vol. 2018, Jun. 2018, Art. no. 4606780.
[13] H. Ren, H. Zhang, H. Zhou, P. Zhang, X. Lei, G. Deng, and B. Hou, "A novel constant output powers compound control strategy for variable-speed variable-pitch wind turbines," *IEEE Access*, vol. 6, pp. 17050–17059, 2018.
[14] A. Dahbi, N. Nait-Said, and M.-S. Nait-Said, "A novel combined MPPT-pitch angle control for wide range variable speed wind turbine based on neural network," *Int. J. Hydrogen Energy*, vol. 41, no. 22, pp. 9427–9442, Jun. 2016.
[15] X. Tang, M. Yin, C. Shen, Y. Xu, Z. Y. Dong, and Y. Zou, "Active power control of wind turbine generators via coordinated rotor speed and pitch angle regulation," *IEEE Trans. Sustain. Energy*, vol. 10, no. 2, pp. 822–832, Apr. 2019.
[16] M. Gholami, S. H. Fathi, J. Milimonfared, and Z. Chen, "Improving power smoothing and performance of pitch angle system for above rated speed range in wind power systems," *IET Gener., Transmiss. Distrib.*, vol. 13, no. 3, pp. 409–416, Feb. 2019.
[17] M. Ben Smida and A. Sakly, "Smoothing wind power fluctuations by particle swarm optimization-based pitch angle controller," *Trans. Inst. Meas. Control*, vol. 41, no. 3, pp. 647–656, Feb. 2019.
[18] D. Wenzhong Gao, X. Wang, J. Wang, T. Gao, M. Stefanovic, and X. Li, "Optimal pitch control design with disturbance rejection for the controls advanced research turbine," *J. Sol. Energy Eng.*, vol. 141, no. 1, Feb. 2019, Art. no. 011005.
[19] H. Mahvash, S. A. Taher, M. Rahimi, and M. Shahidehpour, "Enhancement of DFIG performance at high wind speed using fractional order PI controller in pitch compensation loop," *Int. J. Electr. Power Energy Syst.*, vol. 104, pp. 259–268, Jan. 2019.
[20] H. Mahvash, S. A. Taher, and M. Shahidehpour, "Fractional order control scheme in pitch control loop of synchronous generator wind turbine type 4 at high wind speed operation in a microgrid," *J. Renew. Sustain. Energy*, vol. 11, no. 1, Jan. 2019, Art. no. 013305.
[21] U. Elosegui, I. Egana, A. Ulazia, and G. Ibarra-Berastegi, "Pitch angle misalignment correction based on benchmarking and laser scanner measurement in wind farms," *Energies*, vol. 11, no. 12, Dec. 2018, Art. no. 3357.
[22] R. Ettouil, K. Chabir, and M. N. Abdelkrim, "Synergetic fault-tolerant control for pitch control of wind turbine system," *Electr. Eng.*, vol. 100, no. 4, pp. 2527–2535, Dec. 2018.
[23] C.-S. Wang and M.-H. Chiang, "A novel pitch control system of a large wind turbine using Two-Degree-of-Freedom motion control with feedback linearization control," *Energies*, vol. 9, no. 10, Oct. 2016, Art. no. 791.
[24] H. Habibi, H. R. Nohooji, and I. Howard, "Adaptive PID control of wind turbines for power regulation with unknown control direction and actuator faults," *IEEE Access*, vol. 6, pp. 37464–37479, 2018.
[25] Z. Liu, X. Liu, K. Wang, Z. Liang, J. A. F. O. Correia, and A. De Jesus, "GA-BP neural network-based strain prediction in full-scale static testing of wind turbine blades," *Energies*, vol. 12, no. 6, Mar. 2019, Art. no. 1026.
[26] Y. Zhang, B. Chen, Y. Zhao, and G. Pan, "Wind speed prediction of IPSO-BP neural network based on lorenz disturbance," *IEEE Access*, vol. 6, pp. 53168–53179, 2018.
[27] J. Fan, J. Zhong, J. Zhao, and Y. Zhu, "BP neural network tuned PID controller for position tracking of a pneumatic artificial muscle," *Technol. Health Care*, vol. 23, no. s2, pp. S231–S238, Jun. 2015.
[28] F. Jin, J. Sun, and H. Yu, *Current Development of Mechanical Engineering and Energy*, vols. 494–495. Feb. 2014, pp. 223–228.
[29] D. Xia, L. Kong, Y. Hu, and P. Ni, "Silicon microgyroscope temperature prediction and control system based on BP neural network and fuzzy-PID control method," *Meas. Sci. Technol.*, vol. 26, no. 2, Feb. 2015, Art. no. 025101.
[30] H. Laghridat, A. Essadki, and T. Nasser, "Comparative analysis between PI and linear-ADRC control of a grid connected variable speed wind energy conversion system based on a squirrel cage induction generator," *Math. Problems Eng.*, vol. 2019, pp. 1–16, Mar. 2019.
[31] K. Guo, Y. Pan, and H. Yu, "Composite learning robot control with friction compensation: A neural network-based approach," *IEEE Trans. Ind. Electron.*, vol. 66, no. 10, pp. 7841–7851, Oct. 2019.
[32] S. Li and J. Li, "Output predictor-based active disturbance rejection control for a wind energy conversion system with PMSG," *IEEE Access*, vol. 5, pp. 5205–5214, 2017.
[33] A. Xia, G. Hu, Z. Li, D. Huang, and F. Wang, "Self-optimizing pitch control for large scale wind turbine based on ADRC," in *Proc. 5th Annu. Int. Conf. Mater. Sci. Environ. Eng.*, Xiamen, China, Feb. 2018, vol. 301, no. 1, Art. no. 012155.
[34] X. Anjun, L. Xu, H. Shuju, L. Nianhong, and X. Honghua, "A new pitch control method for large scale wind turbine based on ADRC," in *Proc. Int. Conf. Mater. Renew. Energy Environ.*, Chengdu, China, vol. 1, Aug. 2013, pp. 373–376.
[35] H. Coral-Enriquez, J. Cortés-Romero, and A. Germán Ramos, "Robust active disturbance rejection control approach to maximize energy capture in variable-speed wind turbines," *Math. Probl. Eng.*, vol. 2013, May 2013, Art. no. 396740.
[36] G. Mandic, A. Nasiri, E. Muljadi, and F. Oyague, "Active torque control for gearbox load reduction in a variable-speed wind turbine," *IEEE Trans. Ind. Appl.*, vol. 48, no. 6, pp. 2424–2432, Nov. 2012.
[37] Y. Xiao, Y. Hong, X. Chen, and W. Huo, "Switching control of wind turbine sub-controllers based on an active disturbance rejection technique," *Energies*, vol. 9, no. 10, 2016, Art. no. 793.
[38] K. Guo, Y. Pan, D. Zheng, and H. Yu, "Composite learning control of robotic systems: A least squares modulated approach," *Automatica*, vol. 111, Jan. 2020, Art. no. 108612.

HAIJUN REN received the Ph.D. degree in mechanical engineering from Chongqing University, Chongqing, China, in 2011.

From 2011 to 2014, he was a Lecturer with the School of Automation, Chongqing University of Posts and Telecommunications, China. Since 2015, he has been an Associate Professor with the School of Advanced Manufacture Engineering, Chongqing University of Posts and Telecommunications. From 2015 to 2016, he was a Visiting Scholar with the Institute of Industrial Science, The University of Tokyo.

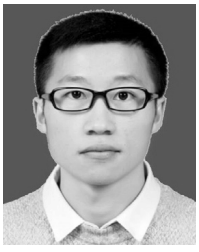

BIN HOU received the B.E. degree in mechanical engineering from the Tianjin University of Technology, Tianjin, China, in 2017. He is currently pursuing the M.S. degree with the School of Advanced Manufacture Engineering, Chongqing University of Posts and Telecommunications, China.

GAO ZHOU received the B.E. degree in electrical engineering and its automation from the University of South China, Hengyang, China, in 2018. He is currently pursuing the M.S. degree with the School of Advanced Manufacture Engineering, Chongqing University of Posts and Telecommunications, China.

CHONG WEI received the B.E. degree in mechanical engineering from the Chongqing University of Posts and Telecommunications, Chongqing, China, in 2019, where he is currently pursuing the M.S. degree with the School of Advanced Manufacture Engineering.

LI SHEN received the B.E. degree in mechanical engineering from the Chongqing University of Posts and Telecommunications, Chongqing, China, in 2019, where he is currently pursuing the M.S. degree with the School of Advanced Manufacture Engineering.

QI LI received the B.E. degree in mechanical engineering from the Chongqing University of Posts and Telecommunications, Chongqing, China, in 2019, where he is currently pursuing the M.S. degree with the School of Advanced Manufacture Engineering.